Nanostructures

DOI: 10.1002/ange.201311309

Two-Dimensional CuSe Nanosheets with Microscale Lateral Size: Synthesis and Template-Assisted Phase Transformation**

*Xue-Jun Wu, Xiao Huang, Juqing Liu, Hai Li, Jian Yang, Bing Li, Wei Huang, and Hua Zhang**

Abstract: *Semiconducting nanosheets with microscale lateral size are attractive building blocks for the fabrication of electronic and optoelectronic devices. The phase-controlled chemical synthesis of semiconducting nanosheets is of particular interest, because their intriguing properties are not only related to their size and shape, but also phase-dependent. Herein, a facile method for the synthesis of phase-pure, microsized, two-dimensional (2D) CuSe nanosheets with an average thickness of approximately 5 nm is demonstrated. These hexagonal-phased CuSe nanosheets were transformed into cubic-phased $Cu_{2-x}Se$ nanosheets with the same morphology simply by treatment with heat in the presence of Cu^{I} cations. The phase transformation, proposed to be a template-assisted process, can be extended to other systems, such as CuS and $Cu_{1.97}S$ nanoplates. Our study offers a new method for the phase-controlled preparation of 2D nanomaterials, which are not readily accessible by conventional wet-chemical methods.*

Two-dimensional (2D) nanomaterials, with the rise of graphene, have drawn tremendous attention because of their unique properties associated with their small thickness and 2D morphology.[1–3] In particular, transition-metal dichalcogenide (e.g. MoS_2, WS_2, TiS_2) nanosheets,[4–8] CdSe nanoplatelets,[9–12] and other 2D chalcogenide nanomaterials[13–15] have been extensively studied and applied in various applications, including field-effect transistors, lithium-ion batteries, gas sensors, and electrocatalysis.

Copper selenide, a typical and important anisotropic p-type semiconductor, has a lot of phases, including stoichiometric (e.g. CuSe, Cu_2Se, Cu_2Se_3) and nonstoichiometric phases (i.e. $Cu_{2-x}Se$). For example, CuSe with a hexagonal phase is stable at room temperature and is commonly used as the precursor for the synthesis of chalcopyrite $CuInSe_2$-based nanostructures.[16,17] $Cu_{2-x}Se$ generally shows a cubic structure, and at $x = 0.2$ has both a direct and an indirect band gap of 2.2 and 1.4 eV, respectively, which are well within the range of ideal band gaps for solar-cell applications.[18] However, the synthesis of 2D copper selenide nanostructures has rarely been reported. For example, free-standing CuSe nanoplates were prepared through a hydrothermal method or a solution-based route,[19,20] but they showed a large size distribution and irregular shapes with a typical thickness of more than 20 nm. Recently, cubic-phased $Cu_{2-x}Se$ nanoplates have been synthesized.[21,22] Unfortunately, their diameter is very small, typically less than 20 nm. Therefore, a novel synthetic strategy to prepare 2D copper selenide with the desired morphology and phase as well as a large lateral size has become urgent in materials science and synthetic chemistry.

Herein, we report a facile, phosphine-free, low-temperature method for the preparation of microscale, phase-pure CuSe nanosheets. Importantly, for the first time, we reveal that the synthesized CuSe nanosheets with a hexagonal phase can be transformed into $Cu_{2-x}Se$ with a cubic phase through simple treatment with heat without damaging the shape of the original 2D nanosheets.

In a typical experiment, a CuSe nanosheet was synthesized through a hot-injection method. To avoid the use of a toxic, pyrophoric, and expensive alkyl phosphine, Se powder was dissolved in a mixture of dodecanethiol (DDT) and oleylamine (OM) as the Se precursor, a method first adopted by the Zhang research group.[23] To initiate the phase transformation, we injected the as-prepared CuSe nanosheet suspension into a hot solution of Cu^{I} in OM at 160 °C for 15 min (see the Supporting Information for experimental details).

Powder X-ray diffraction (XRD) patterns were used to determine the phase composition of the as-synthesized product. All diffraction peaks could be indexed to hexagonal CuSe with the klockmannite structure (JCPDS No. 34-0171) with cell parameters of $a = b = 3.939$ Å and $c = 17.250$ Å (Figure 1a). The hexagonal CuSe nanocrystals were highly oriented, as the (006) planes showed stronger reflection as compared to that in the standard XRD pattern. The

[*] Dr. X.-J. Wu, Dr. X. Huang, Dr. J. Q. Liu, Dr. H. Li, J. Yang, Prof. Dr. H. Zhang
School of Materials Science and Engineering
Nanyang Technological University
50 Nanyang Avenue, Singapore 639798 (Singapore)
E-mail: HZhang@ntu.edu.sg
hzhang166@yahoo.com
Homepage: http://www.ntu.edu.sg/home/hzhang/
Dr. J. Q. Liu, Prof. Dr. W. Huang
Singapore-Jiangsu Joint Research Center for Organic/Bio-Electronics and Information Displays
Institute of Advanced Materials (IAM), Nanjing Tech University
Nanjing 211816 (China)
Dr. B. Li
Institute of Materials Research and Engineering
A*STAR (Agency for Science, Technology and Research)
3 Research Link, Singapore 117602 (Singapore)

[**] This research was supported by MOE under AcRF Tier 2 (ARC 26/13, No. MOE2013-T2-1-034), AcRF Tier 1 (RG 61/12, RGT18/13, and RG5/13), and a Start-Up Grant (M4080865.070.706022) in Singapore. This research was also conducted as part of the NTU-HUJ-BGU Nanomaterials for Energy and Water Management Program of the Campus for Research Excellence and Technological Enterprise (CREATE), which is supported by the National Research Foundation, Prime Minister's Office, Singapore.

Supporting information for this article is available on the WWW under http://dx.doi.org/10.1002/anie.201311309.

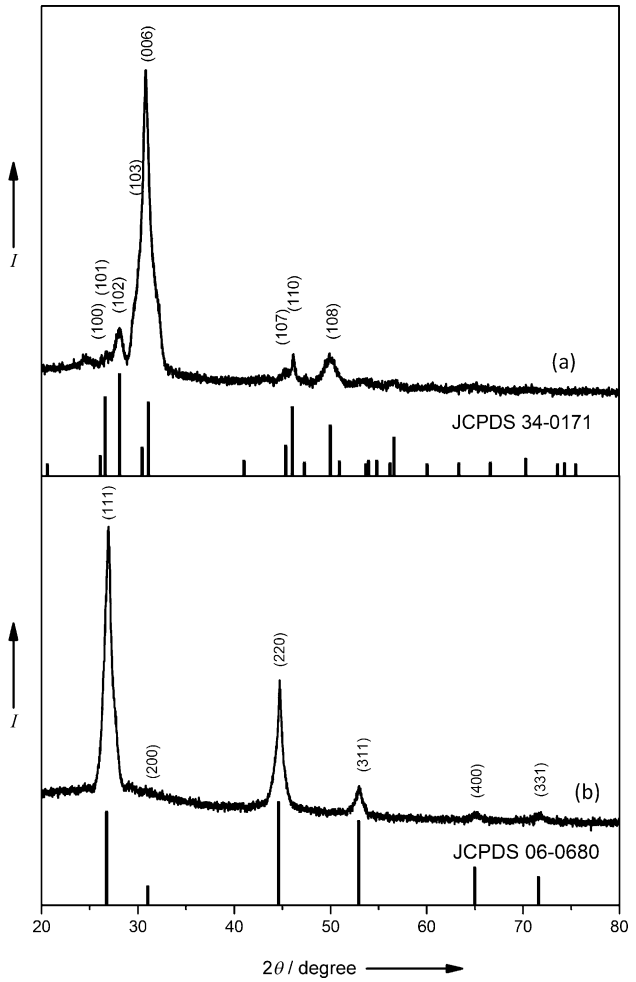

Figure 1. XRD patterns of as-synthesized a) hexagonal CuSe nanosheets and b) cubic $Cu_{2-x}Se$ nanosheets.

diffraction peaks of the copper selenide nanocrystals after further heat treatment in the presence of Cu^I (Figure 1b) were assigned to (111), (200), (220), (311), (400), and (331) planes of cubic $Cu_{2-x}Se$ with the berzelianite structure (JCPDS No. 06-0680). These data suggest that the nanocrystals were successfully transformed from hexagonal CuSe into cubic $Cu_{2-x}Se$. X-ray photoelectron spectroscopy (XPS) data confirmed the change in binding energy of Cu 2p and Se 3d during this transformation (see Figure S1 in the Supporting Information).

Field emission scanning electron microscopy (FESEM) and transmission electron microscopy (TEM) images (Figure 2a,b) show that the as-synthesized 2D CuSe nanocrystals are hexagonal or triangular in shape with an average lateral size of 0.6–1.6 μm. The CuSe nanosheets are quite thin, as deduced from their low contrast in the TEM image (Figure 2b) and the Moiré patterns formed by the stacked layers (see Figure S2a). Therefore, the nanosheets are highly flexible and easy to fold at the edge (see Figure S2b). The high-resolution TEM (HRTEM) images (Figure 2c,d) of a typical CuSe nanosheet show lattice patterns that match well with a crystalline klockmannite structure. The observed interplanar distances between lattice fringes are 0.34 and

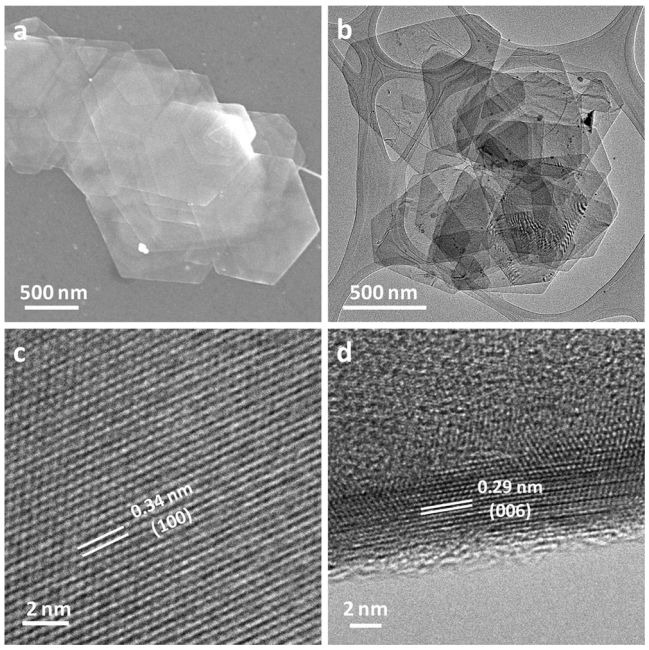

Figure 2. a) FESEM and b) TEM images of as-prepared CuSe nanosheets. c,d) HRTEM images of a small region of a CuSe nanosheet oriented normal to the [001] zone axis (c) and the folded edge of a CuSe nanosheet (d).

0.29 nm, which are consistent with the (100) and (006) planes of hexagonal CuSe, respectively, thus indicating that the CuSe nanosheets grew preferably normal to the [001] direction. The thickness of a typical CuSe nanosheet is about 5.2 nm (Figure 2d), which corresponds to three unit cells (the lattice constant of CuSe along the *c* axis is 1.725 nm). Energy-dispersive X-ray spectroscopy (EDS) data show that the nanosheets are composed of Cu and Se, and the measured Cu/Se molar ratio also confirms the formation of a stoichiometric CuSe compound (see Figure S3).

After the CuSe nanosheets were transformed into $Cu_{2-x}Se$ by simple treatment with heat in the presence of Cu^I, the 2D morphology of the nanocrystals remained unchanged (Figure 3a). The Cu/Se molar ratio was increased to about 2, as indicated by the EDS measurement (see Figure S4). Figure 3b shows the TEM image of a typical $Cu_{2-x}Se$ nanosheet with a lateral size of about 1.6 μm. The selected-area electron diffraction (SAED) pattern of the nanosheet (inset of Figure 3b) reveals its hexagonal symmetry and shows the diffracted spots of {220} planes with a *d* spacing of 0.20 nm, thus indicating that the cubic-phased nanosheets are oriented along the [111] zone axis. We analyzed HRTEM images of the $Cu_{2-x}Se$ nanosheets to further characterize their crystal structure (Figure 3c,d). As shown by the selected-area fast Fourier transform (FFT) pattern and inverse FFT image (Figure 3e,f), the intersecting planes with a *d* spacing of 0.20 nm and dihedral angle of 60° are assignable to {220} planes viewed along the [111] zone axis. From the HRTEM image of the folded edge of a nanosheet (Figure 3d,h), the *d* spacings of the perpendicular planes were measured to be 0.33 and 0.20 nm, which are in good agreement with those of the {111} and {220} planes of the cubic phase, respectively. The

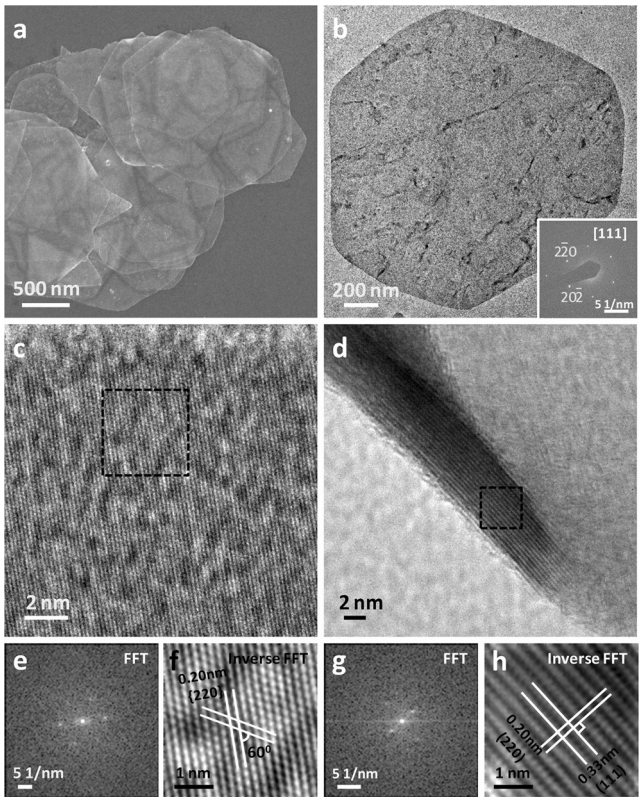

Figure 3. a) FESEM image of $Cu_{2-x}Se$ nanosheets. b) TEM image of a typical $Cu_{2-x}Se$ nanosheet. Inset: SAED pattern of this nanosheet. c, d) HRTEM images of a small region of a $Cu_{2-x}Se$ nanosheet oriented normal to the [111] zone axis (c) and the folded edge of a $Cu_{2-x}Se$ nanosheet (d). e, g) FFT and f, h) inverse FFT images of the areas inside the dashed squares in (c, d), respectively.

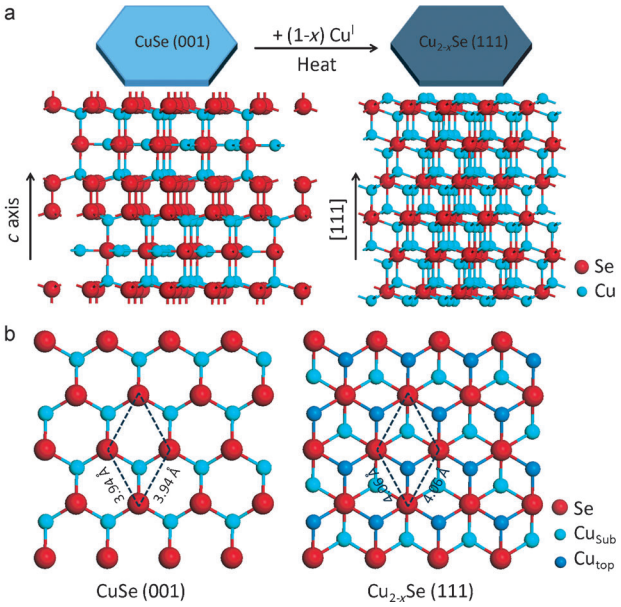

Figure 4. a) Structural models of klockmannite CuSe (left) and antifluorite $Cu_{2-x}Se$ (right). The insertion of additional Cu^{I} into the klockmannite CuSe lattice under heat treatment results in the phase transformation from hexagonal CuSe to cubic $Cu_{2-x}Se$. b) Cu and Se atomic arrangements viewed along the $[001]_{CuSe}$ (left) and $[111]_{Cu_{2-x}Se}$ projection (right).

thickness of the $Cu_{2-x}Se$ nanosheets is approximately 6 nm and thus slightly larger than that of the initial hexagonal-phased CuSe nanosheets (ca. 5 nm). Atomic force microscopy (AFM) images also confirmed the thickness change during the transformation (see Figure S5).

To the best of our knowledge, $Cu_{2-x}Se$ nanosheets have not previously been synthesized from CuSe nanosheets as the starting material through simple heat treatment in the presence of Cu^{I}. In the absence of Cu^{I}, treatment with heat did not induce the phase transformation of CuSe nanosheets, but caused the stacked nanosheets to fuse together into microscale crystals (see Figure S6). To explore the transformation mechanism, we considered the structures of klockmannite CuSe and antifluorite $Cu_{2-x}Se$ (Figure 4). Hexagonal CuSe consists of alternating $CuSe_3$–Cu_3Se–$CuSe_3$ layers and Se–Se van der Waals layers along the *c* (or *z*) axis (Figure 4a, left).[24] On the other hand, cubic $Cu_{2-x}Se$ has an antifluorite structure with the space group $F\bar{4}3m$. A number of structural models have been proposed for $Cu_{2-x}Se$ owing to the complex atomic arrangement of the Cu cations.[25,26] For simplicity, the ideal antifluorite structure with Cu ions located at the tetrahedral interstices of the 8(c) site of Se (see Figure S7) was used as the structural model for $Cu_{2-x}Se$ in the present study (Figure 4a, right).[25] Similarities were found between the CuSe and $Cu_{2-x}Se$ structures. The Se atoms in both the $(001)_{CuSe}$ and the $(111)_{Cu_{2-x}Se}$ planes are hexagonal-close-packed (Figure 4b), whereby the side lengths of the unit parallelograms of $(001)_{CuSe}$ (3.94 Å) and $(111)_{Cu_{2-x}Se}$ (4.06 Å) are very close, and the mismatch between $\{110\}_{CuSe}$ ($d = 1.970$ Å) and $\{220\}_{Cu_{2-x}Se}$ ($d = 2.03$ Å) was calculated to be only 3.0%. The most distinct difference between these two structures is that, as compared to CuSe, more Cu cations are inserted into the interstices of the tetrahedral sites of Se in $Cu_{2-x}Se$, in which two hexagonal-close-packed Cu layers (labeled as Cu_{top} and Cu_{sub} in Figure 4) exist between neighboring Se(111) planes. Therefore, the low occupancy of Cu cations in CuSe and the Se–Se layers bound by van der Waals forces make CuSe an effective structural template for the further insertion of Cu cations and the formation of $Cu_{2-x}Se$. Cu cations have high mobility and ionic diffusivity at high temperature,[27,28] and hence the inserted Cu cations moved rapidly and occupied the interstices with the lowest energy, along with the simultaneous site regulation of pre-existing Cu cations. During this process, whereas the Cu ions diffuse like a "liquid",[27] the Se superlattice acts as a crystalline framework to stabilize the entire structure with unaltered overall 2D morphology. Because of the insertion of Cu cations, the lattice along the *c* axis expanded by about 16%, from $d_{\{006\}}(CuSe) = 2.875$ Å to $d_{\{111\}}(Cu_{2-x}Se) = 3.330$ Å, which explains the observed increase in the nanosheet thickness from the initial value of approximately 5 nm to the final thickness of approximately 6 nm. The lateral size of the nanosheets, however, increased by only about 3%.

It was found that the addition of DDT was critical for maintaining the structural integrity of the nanosheets. Without DDT, the template-based transformation also occurred, but some of the nanosheets were damaged: Etched holes

appeared at the edges together with the formation of small nanoparticles (see Figure S8). These undesired effects occur because the active edges and surface defects of the nanosheets readily react with the Cu^{I} in the solution. In the presence of DDT molecules, which can strongly interact with Cu atoms and bind to them, the surface of the nanosheets is well-stabilized and protected during the insertion of Cu cations into the CuSe templates. Remarkably, our templated transformation strategy can also be applied to other materials, such as CuS, which has a similar hexagonal structure to that of CuSe. Thus, CuS was successfully transformed into $Cu_{1.97}S$ with the djurleite structure (see Figures S9 and S10).

To investigate the property changes of the nanosheets upon the phase transformation from CuSe to $Cu_{2-x}Se$, we acquired and compared UV/Vis/NIR absorption spectra of the two materials (Figure 5a). The absorption spectrum of the CuSe nanosheets presents a strong absorption peak at 712 nm

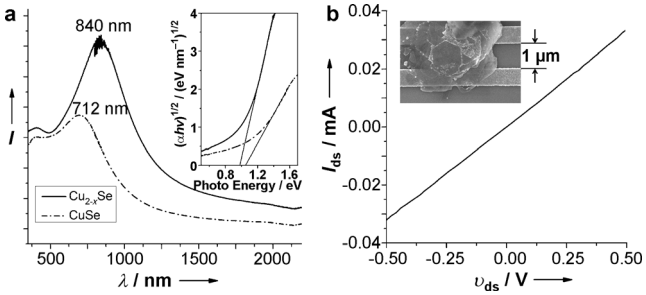

Figure 5. a) UV/Vis/NIR absorption spectra (converted from diffuse reflectance spectra) of CuSe and $Cu_{2-x}Se$ nanosheets. Inset: Corresponding plots of $(\alpha h\nu)^{1/2}$ versus photoenergy ($h\nu$). b) *I–V* curve for the $Cu_{2-x}Se$ nanosheets. Inset: SEM image of the device tested. I_{ds} and V_{ds} are the drain-to-source current and voltage, respectively.

and a weak absorption peak at 404 nm. The corresponding peaks for the $Cu_{2-x}Se$ nanosheets, as compared to those of CuSe, are red-shifted to 840 and 411 nm, respectively. The absorption at short and long wavelengths in both materials can be assigned to direct and indirect interband transitions, respectively.[29,30] To estimate the band-gap energies of both copper selenides, we employed a classical Tauc approach based on the equation $\alpha h\nu = A(h\nu - E_g)n$, in which α, h, ν, and E_g are the absorption coefficient, Planck constant, optical frequency, and the band-gap energy, respectively, whereas A and n are constant ($n = 1/2$ for a direct transition and $n = 2$ for an indirect transition).[31] The absorption coefficient α can be calculated by using the Kubelka–Munk function: $F(R) = \alpha/s = (1-R)^2/(2R)$, in which s is the scattering coefficient and R is reflectance.[32] By using this method, we calculated the indirect band gaps of CuSe and $Cu_{2-x}Se$ nanosheets as 1.05 and 0.98 eV, respectively. These values are suitable for solar-cell applications as well as photoelectric devices in the near-infrared range. The strong absorption peaks in both copper selenides were also recently assigned to localized surface plasmon resonance (LSPR).[33–35] Besides their optical properties, we also measured the electronic properties of the $Cu_{2-x}Se$ nanosheets. Figure 5b shows the current–voltage (*I–V*) behavior of the $Cu_{2-x}Se$ nanosheets between two gold electrodes with a channel width of about 1 μm. The *I–V* curve recorded under ambient conditions shows the ohmic response and high conductivity, which may arise from the large number of copper vacancies spontaneously formed when the nanosheets are exposed to air.[36]

In summary, we have successfully synthesized microsized CuSe nanosheets by using a facile, phosphine-free, low-temperature method. The CuSe nanosheets can be further transformed into cubic $Cu_{2-x}Se$ nanosheets without a morphology change through simple heat treatment in the presence of Cu^{I} cations. A possible mechanism is proposed to explain the phase transformation, which was also demonstrated in other systems. We believe these microsized semiconducting nanosheets are promising building blocks for the construction of various devices, such as sensors and solar cells.

Received: December 31, 2013
Revised: March 12, 2014
Published online: April 7, 2014

Keywords: chalcogenides · copper selenide · nanomaterials · phase transformation · template synthesis

[1] A. K. Geim, *Science* **2009**, *324*, 1530–1534.
[2] a) X. Huang, X. Qi, F. Boey, H. Zhang, *Chem. Soc. Rev.* **2012**, *41*, 666–686; b) X. Huang, Z. Y. Yin, S. X. Wu, X. Y. Qi, Q. Y. He, Q. C. Zhang, Q. Y. Yan, F. Boey, H. Zhang, *Small* **2011**, *7*, 1876–1902; c) X. Huang, Z. Y. Zeng, Z. X. Fan, J. Q. Liu, H. Zhang, *Adv. Mater.* **2012**, *24*, 5979–6004; d) Q. Y. He, S. X. Wu, Z. Y. Yin, H. Zhang, *Chem. Sci.* **2012**, *3*, 1764–1772.
[3] X. Li, X. Wang, L. Zhang, S. Lee, H. Dai, *Science* **2008**, *319*, 1229–1232.
[4] M. Chhowalla, H. Shin, S. G. Eda, L.-J. Li, K. P. Loh, H. Zhang, *Nat. Chem.* **2013**, *5*, 263–275.
[5] a) X. Huang, Z. Zeng, H. Zhang, *Chem. Soc. Rev.* **2013**, *42*, 1934–1946; b) X. Huang, C. L. Tan, Z. Y. Yin, H. Zhang, *Adv. Mater.* **2014**, DOI: 10.1002/adma.201304964.
[6] B. Radisavljevic, A. Radenovic, J. Brivio, V. Giacometti, A. Kis, *Nat. Nanotechnol.* **2011**, *6*, 147–150.
[7] a) Z. Zeng, Z. Yin, X. Huang, H. Li, Q. He, G. Lu, F. Boey, H. Zhang, *Angew. Chem.* **2011**, *123*, 11289–11293; *Angew. Chem. Int. Ed.* **2011**, *50*, 11093–11097; b) Z. Y. Zeng, T. Sun, J. X. Zhu, X. Huang, Z. Y. Yin, G. Lu, Z. X. Fan, Q. Y. Yan, H. H. Hng, H. Zhang, *Angew. Chem.* **2012**, *124*, 9186–9190; *Angew. Chem. Int. Ed.* **2012**, *51*, 9052–9056; c) Z. Y. Zeng, C. L. Tan, X. Huang, S. Y. Bao, H. Zhang, *Energy Environ. Sci.* **2014**, *7*, 797–803.
[8] X. Huang, Z. Zeng, S. Bao, M. Wang, X. Qi, Z. Fan, H. Zhang, *Nat. Commun.* **2013**, *4*, 1444.
[9] S. Ithurria, M. D. Tessier, B. Mahler, R. P. S. M. Lobo, B. Duberter, A. L. Efros, *Nat. Mater.* **2011**, *10*, 936–941.
[10] J. H. Yu, X. Liu, K. E. Kweon, J. Joo, J. Park, K.-T. Ko, D. Lee, S. Shen, K. Tivakornsasithorn, J. S. Son, J.-H. Park, Y.-W. Kim, G. S. Hwang, M. Dobrowolska, J. K. Furdyna, T. Hyeon, *Nat. Mater.* **2010**, *9*, 47–53.
[11] Z. Li, X. Peng, *J. Am. Chem. Soc.* **2011**, *133*, 6578–6586.
[12] Y.-H. Liu, F. Wang, Y. Wang, P. C. Gibbons, W. E. Buhro, *J. Am. Chem. Soc.* **2011**, *133*, 17005–17013.
[13] C. Schliehe, B. H. Juarez, M. Pelletier, S. Jander, D. Greshnykh, M. Nagel, A. Meyer, S. Foerster, A. Kornowski, C. Klinke, H. Weller, *Science* **2010**, *329*, 550–553.
[14] Y. Du, Z. Yin, J. Zhu, X. Huang, X.-J. Wu, Z. Zeng, Q. Yan, H. Zhang, *Nat. Commun.* **2012**, *3*, 1177.

[15] K. H. Park, K. Jang, S. U. Son, *Angew. Chem.* **2006**, *118*, 4724 – 4728; *Angew. Chem. Int. Ed.* **2006**, *45*, 4608 – 4612.
[16] M. Kar, R. Agrawal, H. W. Hillhouse, *J. Am. Chem. Soc.* **2011**, *133*, 17239 – 17247.
[17] M. Ahmadi, S. S. Pramana, L. Xi, C. Boothroyd, Y. M. Lam, S. Mhaisalkar, *J. Phys. Chem. C* **2012**, *116*, 8202 – 8209.
[18] V. M. García, P. K. Nair, M. T. S. Nair, *J. Cryst. Growth* **1999**, *203*, 113 – 124.
[19] G. Xiao, J. Ning, Z. Liu, Y. Sui, Y. Wang, Q. Dong, W. Tian, B. Liu, G. Zou, B. Zou, *CrystEngComm* **2012**, *14*, 2139 – 2144.
[20] X. Liu, X. Duan, P. Peng, W. Zheng, *Nanoscale* **2011**, *3*, 5090 – 5095.
[21] J. Choi, N. Kang, H. Y. Yang, H. J. Kim, S. U. Son, *Chem. Mater.* **2010**, *22*, 3586 – 3588.
[22] H. Shen, H. Wang, H. Yuan, L. Ma, L. S. Li, *CrystEngComm* **2012**, *14*, 555 – 560.
[23] Y. Liu, D. Yao, L. Shen, H. Zhang, X. Zhang, B. Yang, *J. Am. Chem. Soc.* **2012**, *134*, 7207 – 7210.
[24] W. Du, X. Qian, X. Ma, Q. Gong, H. Cao, J. Yin, *Chem. Eur. J.* **2007**, *13*, 3241 – 3247.
[25] A. N. Skomorokhov, D. M. Trots, M. Knapp, N. N. Bickulova, H. Fuess, *J. Alloys Compd.* **2006**, *421*, 64 – 71.
[26] Y. Okada, T. Ohtani, Y. Yokota, Y. Tachibana, K. Morishige, *J. Electron Microsc.* **2000**, *49*, 25 – 29.
[27] H. Liu, X. Shi, F. Xu, L. Zhang, W. Zhang, L. Chen, Q. Li, C. Uher, T. Day, G. J. Snyder, *Nat. Mater.* **2012**, *11*, 422 – 425.
[28] T. Takahashi, O. Yamamoto, F. Matsuyama, Y. Noda, *J. Solid State Chem.* **1976**, *16*, 35 – 39.
[29] H.-L. Li, Y.-C. Zhu, S. Avivi, O. Palchik, J.-P. Xiong, Y. Koltypin, V. Palchik, A. Gedanken, *J. Mater. Chem.* **2002**, *12*, 3723 – 3727.
[30] S. Deka, A. Genovese, Y. Zhang, K. Miszta, G. Bertoni, R. Krahne, C. Giannini, L. Manna, *J. Am. Chem. Soc.* **2010**, *132*, 8912 – 8914.
[31] S. Tsunekawa, T. Fukuda, A. Kasuya, *J. Appl. Phys.* **2000**, *87*, 1318 – 1321.
[32] W. W. Wendlandt, H. G. Hecht, *Reflectance Spectroscopy*, Wiley-Interscience, New York, **1966**, pp. 62.
[33] C. M. Hessel, V. P. Pattani, M. Rasch, M. G. Panthani, B. Koo, J. W. Tunnell, B. A. Korgel, *Nano Lett.* **2011**, *11*, 2560 – 2566.
[34] D. Dorfs, T. Härtling, K. Miszta, N. C. Bigall, M. R. Kim, A. Genovese, A. Falqui, M. Povia, L. Manna, *J. Am. Chem. Soc.* **2011**, *133*, 11175 – 11180.
[35] Y. Xie, L. Carbone, C. Nobile, V. Grillo, S. D'Agostino, F. Della Sala, C. Giannini, D. Altamura, C. Oelsner, C. Kryschi, P. D. Cozzoli, *ACS Nano* **2013**, *7*, 7352 – 7369.
[36] S. C. Riha, D. C. Johnson, A. L. Prieto, *J. Am. Chem. Soc.* **2011**, *133*, 1383 – 1390.

